# A zero dimensional hybrid organic-inorganic perovskite CuCl 4 based: Synthesis, crystal structure, vibrational, optical properties, DFT and TDFT calculations, dielectric properties and biological activity

Aroussia Hachani, Imen Dridi, Abdelhak Othmani, Thierry Roisnel, Stéphane Humbel, Kefi Riadh

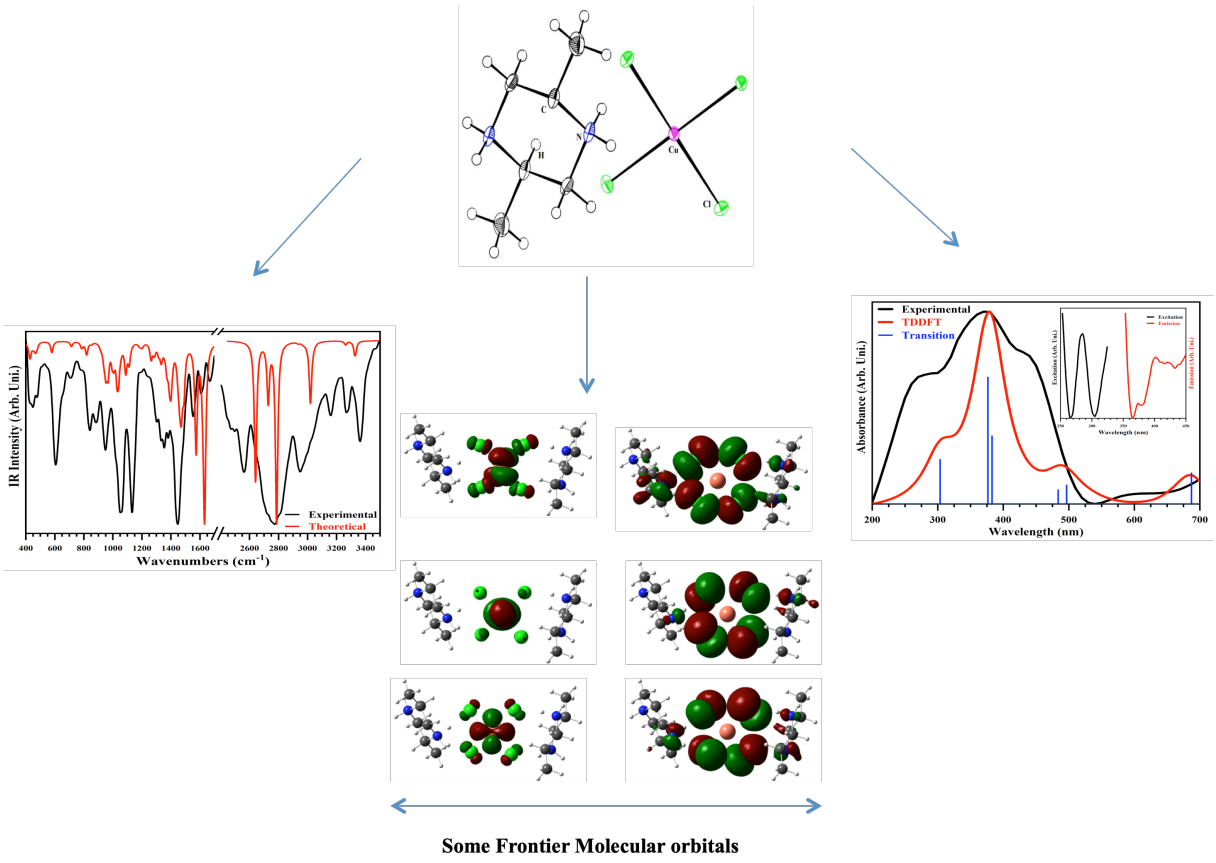


**Some Frontier Molecular orbitals**

# Graphical abstract

# A zero dimensional hybrid organic- inorganic perovskite $CuCl_4$ based: Synthesis, crystal structure, vibrational, optical properties, DFT and TDFT calculations, dielectric properties and biological activity

Aroussia Hachani [a], Imen Dridi [b], Abdelhak Othmani [c], Thierry Roisnel [d], Humbel Stephane [e], Kefi Riadh [a]*

[a] Laboratoire de Chimie des Matériaux, Faculté des Sciences de Bizerte, 7021 Zarzouna, Tunisie.
[b] Laboratory of Biochemistry and Molecular Biology, Faculty of Sciences, Risks Related to Environmental Stress, Struggle and Prevention (UR17ES20), University of Carthage, Te Ministry of Higher Education and Scientifc Research, Zarzouna, 7003 Bizerte, Tunisia.
[c] Laboratoire de Physique des Matériaux, Faculté des Sciences de Bizerte, 7021 Zarzouna, Tunisie.
[d] Univ Rennes, CNRS, ISCR (Institut des Sciences Chimiques de Rennes) – UMR 6226, F-35000 Rennes, France.
[e] Aix-Marseille Université, Centrale Marseille CNRS, iSm2 UMR 7313, 13397 Marseille, France.

**Abstract**

The paper reports the preparation and structural characterization of a new complex $(C_6H_{16}N_2)[CuCl_4]$ grown by slow evaporation technique in aqueous solution and characterized by X-ray diffraction, spectroscopy measurement, DTA-TG analysis, and photoluminescence properties. The crystal structure determination shows that the title compound crystallizes in the C 2/c space group of the monoclinic system. The unit cell dimensions at T=150K are as follows : a = 14.500(5) Å, b = 14.619(5) Å, c = 5.9173(17) Å, β = 107.419(11) °, V = 1196.8(7) $Å^3$ and Z = 4. The atomic arrangement can be described by thick layers of inorganic entities, made up from $CuCl_4$ anions, developed parallel to the (a, c) planes at y = 0 and 1/2. The organic cations are anchored onto successive layers and connect them via N-H...Cl hydrogen bonds, to form an infinite three dimensional network. In addition, the nature and proportion of contacts in the crystal packing were studied by the Hirshfeld surfaces. The vibrational properties were investigated experimentally by means of IR and Raman spectroscopy and theoretically by DFT calculations. Furthermore, the UV-Visible optical absorption and photoluminescence properties were explored by experimental techniques and TDDFT calculations. Good agreement was found between theoretical and

experimental results. Thermal analysis reveals the decomposition of the compound at 511 K. The bioassay results showed that the structure exhibits significant antibacterial activity.

**Keywords:** Complex compound, X-ray single crystal diffraction, , Infrared and Raman spectroscopy, DFT and TDDFT calculations, Optical absorption and photoluminescence measurements, impedance spectroscopy, biological study**.**

## 1. Introduction

Organic-inorganic hybrid materials represent a formidable class of materials that combine the physicochemical properties of organic and inorganic product components into a single compound at molecular scale **[1]**. Concerning the organic part, a diversity of amines has been employed already in the preparation of halocuprates, including aliphatic, aromatic and cyclic amines. In particular, piperazine and its derivatives, have also attracted serious interest amongst crystal engineers, because they are adept to style hydrogen bonds in multiple directions and are adequately harsh cations **[2,3]**. The piperazine nucleus is usually found in biologically active compounds across a number of various therapeutic areas **[4]**. Part of these therapeutic field include antimicrobial, cytotoxic, anticonvulsant, antidepressant, anti-inflammatory, antimalarial, anti-tubercular, antiarrhythmic, antiviral and antioxidant activities etc **[5]**.

As example, the chlorocuprate compounds present an important and interesting class of materials belonging to the large halogenometallate family. In the inorganic component, copper (II) halide complexes have played a significant part in the developments of optoelectronic devices and electronic, laser technology, as well as wireless temperature sensors **[6]** and optical communication **[7]**.

The objective of the article is to synthesize a new copper (II) hybrid trans 2, 5-dimethyl-piperazinium tetrachloridocuprate(II) with general chemical formula $(C_6H_{16}N_2)[CuCl_4]$, and to discuss the results of the structural characterization by X-ray diffraction, Hirshfeld surface, vibrational, optical, thermal properties and biological study. Furthermore, impedance spectroscopy study in the temperature range from 393K to 503K and in the frequency range between 10 and 13 MHz was reported in this work.

## 2. Experimental

### 2.1 Synthesis of $(C_6H_{16}N_2)[CuCl_4]$

The $(C_6H_{16}N_2)[CuCl_4]$ crystals were obtained by dissolving in a concentrated HCl solution a stoichiometric mixture of trans-2,5 dimethylpiperazine and a solution of $CuCl_2.2H_2O$ in a minimum volume of water and stirring for 7h, until the formation of a clear

mixture without any precipitate. Within few weeks, yellow crystals suitable for X-ray investigation were grown.

### 2.2 X-ray single crystal structural analysis

Single crystals were carefully selected under a microscope in order to perform its structural analysis by X-ray diffraction. Data were collected at 150 K on a D8 VENTURE Bruker AXS diffractometer using a mirror monochromatic Mo Kα radiation, λ = 0.71073 Å. The structure was solved by dual-space algorithm using the SHELXT program, and then refined with full-matrix least-square methods based on $F^2$ (SHELXL) **[8]**.

All non-hydrogen atoms were refined with anisotropic atomic displacement parameters. Except nitrogen linked hydrogen atoms that were introduced in the structural model through Fourier difference maps analysis, H atoms were finally included in their calculated positions. A final refinement on $F^2$ with 1367 unique intensities and 69 parameters converged at $\omega R(F^2)$ = 0.069 ($R(F)$ = 0.026) for 1230 observed reflections with $I > 2\sigma(I)$. Crystal data are reported in (Table 1). Drawings were made with Diamond **[9]**.

### 2.3 Physical measurements

The X-ray powder diffraction (PXRD) was carried out on a BRUKER D8 ADVANCE X-ray diffractometer and graphite monochromatic CuKα radiation with a 2θ range from 10 to 40°. The infrared spectra were recorded in the 400–4000 $cm^{-1}$ range with a Nicolet 1000 spectrophotometer, using a sample pressed in spectroscopically pure KBr pellets at ambient temperature. The UV absorption spectrum ~~and diffuse reflectance spectra~~ was measured at room temperature with Perkin Elmer Lamda 35 UV/Vis spectrophotometer in the range of 200-700 nm. Emission spectrum was obtained on a Perkin-Elmer LS55 fluorescence spectrometer equipped with a 450W xenon lamp as the excitation source using solid sample at room temperature. As for the Raman spectra, they were performed at room temperature using a Dilor XY set-up. The ATD-TG analysis curves of the title compound was carried under argon atmosphere at a heating rate of 5°/min in the temperature range 310-780 K on a sample of 9.3 mg.

The AC conductivity data and electrical measurements of the real Z' and imaginary Z'' components of the impedance parameters were made over between a range of temperatures (393-503 K) in 10°C intervals. These measurements have been executed by using an HP 4192A impedance analyzer. To assure electrical contacts, the two parallel surfaces of the sample (having a cylindrical shape) were coated by a layer of silver paint. The platinum wires and the sample were held in contact by a weak mechanical pressure controlled by a screw/spring system and transmitted by an alumina rod. The signal frequency ranged

from 10 Hz to 13 MHz. In fact, the sample was pressed into pellets of 12 mm in diameter and 0.6 mm in thickness.

### 2.4 Biological study

The in-vitro antioxidant activity of$(C_6H_{16}N_2)[CuCl_4]$ and trans-2,5 dimethylpiperazine were studied, using two tests diphenylpicrylhydrazyl (DPPH) and (2,2'-azino-bis(3-ethylbenzothiazoline-6-sulfonic acid)) ABTS.

The DPPH activity of $(C_6H_{16}N_2)[CuCl_4]$ and trans-2,5 dimethylpiperazine was studied according to the method [**10**] as described in [**11**]. Briefly, different concentrations ranging between (0.5 and 50 mg/ml) for $(C_6H_{16}N_2)[CuCl_4]$, (0.1 and 2.5 mg/ml) for trans-2,5 dimethylpiperazine were prepared. Both the tested compounds were dissolved on methanol. Three milliliters of DPPH methanol solution (0.1mM) were added to 100µl of $(C_6H_{16}N_2)[CuCl_4]$ and trans-2,5 dimethylpiperazine solution. After 30 min of incubation at room temperature and on the obscurity, the absorbance was measured at 517 nm. All samples were tested in triplicate. The scavenging activity was determined according to the following formula: DPPH radicals scavenged activity (%) = $[(A_0 - A_1)/A_0] \times 100$.

Where $A_0$ refers to the absorbance of the blank and $A_1$ refers to the absorbance measured in the presence of $(C_6H_{16}N_2)[CuCl_4]$ or trans-2,5 dimethylpiperazine.

ABTS test is based on color change of the ABTS cation after its reaction with an antioxidant. Indeed, ABTS is converted into its radical cation, having a blue color, after reacting with potassium persulfate. The reaction of ABTS cation with an antioxidant, frequently, leads to ABTS colorless form. The color change is measured by spectrophotometry. To perform the ABTS test, an equal volume of 7 mM ABTS solution and 2.45 mM potassium persulfate solution were mixed to prepare a stock solution. After incubation, for 12 h at room temperature in the dark, a working solution is freshly prepared, before each essay, by mixing an equal volume of the stock solution and methanol (50%). Different concentrations ranging between (10 and 20 mg/ml) for $(C_6H_{16}N_2)[CuCl_4]$, (0.1 and 10 mg/ml) for trans-2,5 dimethylpiperazine were prepared. Three milliliter of ABTS working solution were added to 300 µl of $(C_6H_{16}N_2)[CuCl_4]$ and trans-2,5 dimethylpiperazine. The mixture was incubated, in the dark and at room temperature, for 6 min. Then the absorbance was measured at 734 nm [**11, 12**]. For each concentration, data are recorded in triplicate. The scavenging activity was estimated based on the formula as bellow:

ABTS radicals scavenged activity (%) = $[(A_0 - A_1)/A_0] \times 100$. Where $A_0$ is the absorbance of the blank (the reaction mixture without the tested compound) and $A_1$ is the absorbance measured in the presence of the tested compound.

The antibacterial activity of $(C_6H_{16}N_2)[CuCl_4]$ and trans-2,5 dimethylpiperazine were tested against 4 bacteria including one gram-positive bacteria: *Staphylococcus aureus* NCTC 6571 and three gram-negative bacteria, namely *Escherichia coli* JW 1772, *Salmonella typhimurium* ATCC 14028 and *Pseudomonas aeruginosa* SH 38 as recommended by the Clinical Laboratory Standards Institute [**11**]. After growing bacterial strains overnight on nutrient broth at 37º C, 100µl of each tested bacteria suspension, containing $10^7$ colony-forming units (cfu/ml), were placed on the surface of sterile agar plates. 6 mm of diameter sterile discs (Whatman filter paper No.1), were soaked with 10µl of $(C_6H_{16}N_2)[CuCl_4]$ and trans-2,5 dimethylpiperazine dissolved in Dimethyl sulfoxide (DMSO) (1 mg/mL). For the negative controls, dimethylsulfoxide (DMSO) was used instead. Impregnated discs were then placed on inoculated plates. The plates were inverted and incubated for 24 h at 37°C. Inhibition zones were measured in mm. Each test was performed twice in triplicate.

## 3. Computational details

The theoretical study conducted in this work consists of DFT and TDDFT calculations of the vibrational and optical properties of our material, respectively. All the calculations were carried out using Gaussian 09 W program package [**13**] with the B3LYP functional [**14-16**] and using the LANL2DZ basis set [**17**]. Firstly, optimization geometry has been applied on a well chosen cluster from the single crystal RX data. Then, a theoretical study of IR and Raman vibrational modes was carried out and the absence of negative calculated frequencies clearly indicates that the optimized geometry reproduces an equilibrium state and a minimum local energy. Finally, the calculation of the electronic transitions liable to take place between 200 and 700 nm was undertaken on the optimized geometry of the cluster. Throughout this work, the GaussView 5.0 software [**18**] was used to reproduce the theoretical spectra by Lorentzian line shape and through half widths of 10 $cm^{-1}$ for the IR and Raman spectra and of 25 nm for the UV-Visible absorption spectrum. The assignment of the vibrational modes was provided by the visualization of the atoms movements for each calculated frequency with the same software. All the computed frequencies were scaled by 0.961 [**19**] for more reliability with their related experimental vibrational modes.

## 4. Results and discussion

### 4.1 Structure description

The experimental powder X-ray diffraction pattern (PXRD) of $(C_6H_{16}N_2)[CuCl_4]$ is in good agreement with the simulated pattern derived from the atomic coordinates deduced from single crystal diffraction data analysis, indicating the purity and homogeneity of the synthesized product (Fig.1). The trans2,5-dimethyl-piperazinium tetrachloridocuprate(II)

$(C_6H_{16}N_2)[CuCl_4]$ crystallizes in monoclinic space group $C_2/c$ (Z = 4), with a= 14.500(5) Å, b= 14.619(5) Å, c= 5.9173(17) Å, β=107.419(11)° at T=150K, as deduced from X-ray single crystal diffraction study. Configurations of the different organic and inorganic species including the vibrational ellipsoids at 50% probability are depicted in (Fig.2). In the present crystal structure, the molecular components are stabilized through intricate three dimensional hydrogen bonding network as listed in Table 3.

The atomic arrangement can be described by thick layers of inorganic entities, made up from $CuCl_4$ anions and $NH_3$ groups, developed parallel to the (a, c) planes at y = 0 and 1/2 (Fig.3). The organic cations are anchored onto successive layers and connect them via N-H...Cl hydrogen bonds with lengths lying in the range of 2.29 (2) to 2.95Å, with H2A bifurcated, to form an infinite three dimensional network. This structure consists of one-dimensional tubes centre to the axes located at the intersection of the planes (x = 0, y = 1/2) and (x = 1/2, y = 0), linked together so as to form the open framework structure (Fig.4).

The inorganic anion consists of one crystallographical atomic site for Cupper atom (Cu1) linked to four Chlorine atoms in a square planar geometry. The description of $[CuCl_4]^{2-}$ entity is justified by Cu-Cl bonds distances.

The organic molecule, adopt a chair conformation, the interatomic distances C-C and N-C are in the ranges of 1.512(2) - 1.513(3) Å and 1.497(2) -1.498(2) Å respectively. The N-C-C angle value vary from 110.15 (15) to 111.66 (15) °All the bond angles and distances are compared to those found within the hybrid compounds **[20-23]**. The conformation of the piperazine six-membered ring can be described in terms of Cremer and Pople puckering coordinates **[22]**, evaluating the parameters Q (total puckering amplitude), q2, q3, θ and φ. The calculated values are as follows: Q = 0.9467 Å, q2 = 0.9467 Å, q3 = 0.0000 Å, θ = 90° and φ = 159.32°, which correspond to the structure most stable chair conformation.

### 4.2 Hirshfeld surface

In order to analyze the function of the organic base in structural propagation, Hirshfeld surface analyses on $(C_6H_{16}N_2)[CuCl_4]$ were carried out. Hirshfeld surface have been calculated using CRYSTALEXPLORER 3.1 **[24]**. The 3D $D_{norm}$ surfaces are mapped over a fixed color scale of -0.47 to 1.39 Å, shape index mapped within the color range of -1.00 to 1.00 Å, and curvedness in the range of -4.00to 0.40 Å respectively (Fig.5). The 2D fingerprint plots obtained by Hirshfeld surface analysis can classify every type of intermolecular interactions, and their relative contribution can be attained from the area of the surfaces.

The Hirshfeld surface of the asymmetric unit mapped with $d_{norm}$ property, the large circular depressions (deep red) are indicators of hydrogen bonding contacts. The little extent of area

and light colour on the surface indicates weaker and longer contact compared to other hydrogen bonds. The complete fingerprint plot has been derived. 2D fingerprint plots inform not only which interactions are present but also the relative contributions to the Hirshfeld surface. The 2D fingerprint plots were displayed by using the standard view with the $d_e$ and $d_i$ distance scales displayed on the graph axes.

The enrichment ratios of contacts between the different chemical species were computed with software MoProViewer **[25]**, in order to highlight which contacts are statistically favored and are maintaining the crystal packing. Enrichment ratios larger than unity denote contacts which are over-represented in the crystal packing with respect to the chemical composition on the Hirshfeld surface. The hydrophobic Hc atoms bound to carbon were distinguished from the more electropositive H…N and reciprocal contacts XY and YX were merged. The chemical nature of contacts in the crystal structure is shown in Table 4.

Globally, H···Cl/Cl···H, and H···H interactions were most abundant in the crystal packing (58.2, 33.6 % respectively) (Fig. 6). These contacts are attributed to C-H…Cl and N-H…Cl hydrogen bonding interactions and appear as two shape symmetric spikes (1) in the two dimensional fingerprint maps with a prominent long spike at de+di~2.8 Å. They have the important significant contribution to the total Hirshfeld surface (58.2 %) and this type appear with elevated enrichment ECl…HC=1.08 and ECl...HN= 2.80. Then the chlorine and hydrogen atoms are often mutual partners in the crystal contacts and they are electrostatically favorable due to the partial positive charge of H atoms. Furthermore, this type of contacts is important frequent interactions due to the abundance of chlorine and hydrogen on the molecular surface (%SCl=25.85 , % SHC=47 and %SHN=9.48) (Table 4). H...H interactions are the second most frequent interactions, these interactions cover 33.6 % of the total surface and present in the middle of the scattered points in the two-dimensional fingerprint maps with a single broad peak at de=di~1.1 Å, and this type appear with enrichment EHC...HC=2.10. Also the Cl...Cu/Cu...Cl contacts show the presence of scattered points in the middle of the two-dimensional fingerprint maps with a single board peak respectively at de=di~1.6 Å and which represent 5.9 %. These contacts are impoverished in the crystal with a value of enrichment equal to 0.89. Finally, the types of contacts present the stability of the crystal structure and the Cl…H is the driving forces in the molecular arrangement.

### 4.3 Vibrational analysis

In order to give more information on the crystal structure, we have studied the vibrational properties of our compound using Raman scattering and Infrared absorption at room temperature. For more convincing, we used the theoretical results of the DFT

calculations to better attribute the observed vibration modes. Therefore, we present in Fig. 7 and Fig.8 the superimpositions of the experimental and theoretical spectra of the IR and Raman vibrational studies, respectively. In addition, in Table 5, we have gathered assignment attempts of some IR and Raman vibrational modes based mainly on the theoretical results and on previous studies conducted on similar compounds **[26-33]**.

The Raman features observed under 300 $cm^{-1}$ are characteristics of the anionic $[CuCl_4]^{2-}$ as mentioned in literature **[28, 32, 33]**. In effect, the symmetric and asymmetric deformations modes are observed at 115 and 155 $cm^{-1}$, respectively. The intense peaks at 180 and 260 $cm^{-1}$ are assigned respectively to symmetric and asymmetric stretching modes of the CuCl bonds. The Raman peaks calculated at 227 $cm^{-1}$ correspond to the $CH_3$ torsion mode and no related feature is detected experimentally.

The vibrational modes related to the piperazinium cation can be decomposed in several wavenumbers ranges as can be seen in Table 5. We observed separately the angular ring deformation, the rocking, twisting and deformation modes of $NH_2$, $CH_2$ and $CH_3$ groups while the stretching modes were observed between 900 and 1100 $cm^{-1}$. At higher wavenumbers range, the asymmetric and symmetric stretching modes of the hydrogen linked atoms are well defined and assigned. It is worthily noting the relative good agreement observed between the theoretical and experimental vibrational modes for both the Raman and IR techniques. This is well proved with the good correlation between almost all the calculated and observed vibrational wavenumbers depicted in the correlation graph shown in Fig. S1 (The calculated correlation coefficient is 0.999)

### 4.4 Optical Absorption and photoluminescence

The optical properties of the titled compound have been investigated by recording their room-temperature UV-Visible absorption, emission and excitation spectra. TDDFT calculation is also carried out in order to compute the existing electronic transitions wavelengths and to define their natures and to aid in more accurately identifying the observed UV-Visible absorption features. The experimental UV- Vis absorption spectrum superposed with its theoretical homologue is presented in Fig.9. The experimental absorption spectrum of $(C_6H_{16}N_2)[CuCl_4]$ shows a broad band centred at 373 nm (3.32 eV) with an higher and lower energies shoulders at 285 nm (4.35 eV) and 430 nm (2.88 eV), respectively. Also, at more low energies side, we observed an enhancement of the absorption intensities with the detection of a band at 630 nm (1.96 eV) and the presence of additional low energetic transitions referred to the well-known d-d transitions in the orbits of metal ion $Cu^{2+}$. These observed features are typical of CuCl based materials and agree well with similar compounds

[**29-37**]. Worthily, we also reclaim the relatively harmony between experimental and theoretical results, as can be seen in Fig.9. Indeed, the theoretical absorption spectrum shows a band centred at 379 nm and two shoulders on either side at 303 nm and 486 nm. It also proved the presence of computed transitions assigned to d-d transitions at lower energies sides (687 nm). The main assignments of these recorded spectra are regrouped in Table 6.

Theoretically, the calculated transitions between 200 and 700 nm are due to electrons transfers from deep HOMO levels toward the LUMO level only. Based on the 3D representation of the molecular orbitals involved in these transitions (Fig. 10), we notice that all the theoretical absorption features, and therefore those observed experimentally; involved a change in electronic density only within the inorganic $CuCl_4$ part. More precisely, the four highest occupied molecular orbitals (from the HOMO level to the HOMO-3 level) show a charge distribution on the 3d atomic orbitals of Cu and 3p of Cl. Whereas, the HOMO-4 and HOMO-5 levels prove charges distributed only on the 3p atomic orbitals of chlorine. On the other hand, the LUMO level indicates a distribution of charge on the atoms of copper (3d) and chlorine (3p).

Therefore, according to the theoretical results of the assignments gathered in Table 6, we can confirm the fact that the observed shoulder at 430 nm is due to excitonic transitions at the within the $CuCl_4$ planes. Whereas, the intense band around 373 nm and the shoulder on the high energy side at 285 nm, clearly indicate the contribution and the presence of the charge transfer phenomenon between the chlorine atoms and the central copper.

In addition, the band gap of the title compound evaluated using the Tauc plot method **[38]**, and using the Kubelka-Munk function from the reflectance R [$F(R)=(1-R)^2/2R$] is 2.24 eV (Fig. S2). This value indicates that the title compound is a semiconductor with wide band gap **[39]**. Based on this band gap value of 2.24 eV and on the excitonic transitions location at 2.88 eV, we can deduce a value for the exciton binding energy at about 640 meV. This energy is typical of other values presented in the bibliography and clearly proves the great stability of the excitons and the high favorability to recombine and emit intense luminescence that can be seen with the naked eyes even at room temperature. In the present case, under the excitation at 280 nm, the recombination of the electron and the hole in the exciton sends a blue emission at two very close wavelengths; 410 and 430 nm (inset of Fig. 9). Since the organic molecule used is transparent in the visible range, this luminescence comes mainly from the electronic and excitonic transitions within the inorganic anions $[CuCl_4]^{2-}$ **[29, 30, 32]**. Moreover, the excitation spectrum which represents the variation of the intensity of the emission band at 400

nm as a function of excitation wave lengths is reported in (inset of Fig. 9). It exhibits one band with maximum at 285 nm, proves the selected region of the excitation wavelength.

Interestingly, the molecular orbital calculations of these materials show evidence of a powerful tool for the semi quantitative study of some reactivity indices and are very important for assessing stability, chemical hardness and flexibility **[40,41]**. In fact, the ionization energy and electron affinity are expressed using the following relations: I= $-E_{Homo}$ and A= $-E_{LUMO}$. Using the HOMO and LUMO energies, the chemical potential μ, the hardness η, the softness S and the electrophilicity index of the compound are given respectively by the following relations: $\square = \frac{-(I+A)}{2}$, $\square = \frac{(I-A)}{2}$, $S = \frac{1}{2\square}$ and $W = \frac{\square^2}{2\square}$ which are given in Table 7. According to the table, the title compound has a good stability and high chemical hardness (low chemical reactivity) because it is energetically unfavorable to add electron to high-lying LUMO, to extract electrons from low lying HOMO [**42**].

### 4.5 Thermal study

The study of simultaneous thermograms (TG-DTA) was carried out by heating a sample $(C_6H_{16}N_2)[CuCl_4]$ from 310 to 780 K. The profile of the thermograms is presented in Fig.11, illustrates the existence of four distinct anomalies at T1 = 425 K, T2 = 520 K, T3 = 550K, and T4 = 610 K. The first anomaly located at T1 = 425 K, without loss of mass on the signal TG, may be due to a phase transition confirmed by the conductivity measurements. In order to know what type of phase transition is it. we analyzed the compound by DSC technique up to a temperature of 450 K, with recording of the signal during cooling. During this cycle, no thermal accident is detected (Fig.S3), which means that it is an irreversible phase transition of the first order.

The second and third observed respectively at 520 K and 550 K can be assigned to the decomposition of the compound resulting in the successive departure of two molecules of hydrochloric acid, in good agreement with the calculated weight loss [Δm1 (exp) = Δm2 (exp) ≈ (10.75%), Δm1 (theo) = 11.35%]. finally the last broad peak at 680 K corresponds to the degradation of the organic part, confirmed by the presence of black powder mixed with $CuCl_2$ at the end of the experiment.

### 4.6 Complex impedance spectroscopy

**Impedance analysis**

The variation of the imaginary part Z " of the impedance as a function of its real part Z' at different temperatures are given in Fig.12. The curves present as semicircles either passing through or close to the origin were obtained for 393 K to 503 K. The value of the resistance at a given temperature is determined from the intersection of the Nyquist diagram with the abscissa. The equivalent electrical circuit of this sample could be regarded as parallel combination of a bulk resistance Rb and constant phase element CPE. When temperature intensifies, these circles become greatly smaller indicating an activated thermal conduction mechanism **[43].**

The variation of the real part of the complex impedance Z' (Fig.13a) as a function of the frequency at different temperatures shows that the increase of these latter factors leads to the decrease in the values of Z' until it cancel to high frequencies. On the other hand, the spectra Z" = f (log f) giving the variation of the imaginary part Z" (Fig.13b) are characterized by the appearance of the maximums ($f_{max}$, $Z"_{max}$) of which the intensity decreases with increasing temperature which reflects the presence of relaxation phenomenon **[43]**. Each peak is characterized by a maximum frequency $f_{max}$ which decreases in intensity and shifts towards the high frequencies for increasing temperatures. This shows that the relaxation phenomenon depends on the temperature **[44,45].**

**Modulus analysis**

The complex modulus formalism has been used in the analysis of the electrical properties because it gives information about the relaxation mechanism. The electric modulus data are calculated from the real and imaginary parts of the measured impedance data and the pellet dimensions using the following equations: $M' = -\omega C_0 Z''$ ; $M'' = \omega C_0 Z'$ where $C_0 = \varepsilon_0 S/e$ : The frequency dependence of the real and imaginary part M' & M'' of the title material at different temperatures are given respectively in Fig.14 (a,b).

We observed that in the low frequency region the values of M' are very low, which explains why the polarization phenomena due to the interfacial effects and to the electrodes contribute in a negligible way. At high frequencies, the diagrams relating to M" are characterized by the appearance of peaks at a critical frequency $\omega_{max}$ highlighting a relaxation phenomenon. These peaks move to higher frequencies while increasing the temperature.

Fig.15 (a, b) shows respectively the variation of the real part ε' and the imaginary one ε'' of the permittivity as a function of the frequency for different temperatures. The analysis of these diagrams reveals that for low frequencies the permittivity ε' and ε'' increase with the decrease

of the frequency for the temperature differences, which suggests the presence of different types of polarizations and mainly the electrode polarization.

**Conductivity study**

The values of resistance $R_P$ (the intercept of the semicircular arcs of the grain response on the real axis at different temperatures), can be used to obtain the electrical conductivity **σ** defined by the following relation : $\sigma = e/R_P S$ (S is the electrolyte-electrode contact area and **e** is the thickness of the sample) increases with the increase in temperature. In order to understand the conduction phenomena, we used the Arrhenius relation **[46].** The thermal evolution of the specific conductivity Ln(σT) versus (1000/T) is shown in Fig.16 indicating an Arrhenius-type behavior. The Arrhenius diagram proves that there is a change in the conduction mechanism and that our material is not stable in the temperature range [393-503] K because the curves are in the form of two linear branches that check well the law of Arrhenius:

$$\sigma = \frac{A}{T\ exp}\left(\frac{-Ea}{KBT}\right)$$

Two regions associated with two activation energies are observed separated at T = 433 K. Thus, following the Arrhenius law, the obtained activation energies are Ea1 = 1.31 eV in region I between [393- 433] K and Ea2 = -0.08 eV in region II between [433- 503] K. These observations suggested that the conductivity is caused by temperature increase of the protons hoping motion.

## 4.7 Biological study

The result issued from the DPPH test revealed the scavenging activity of trans-2,5 dimethylpiperazine ($IC_{50}$ = 1.83± 0.06 mg/ml) is significantly higher ($p<0.05$) than $(C_6H_{16}N_2)[CuCl_4]$ ($IC_{50}$ = 49.05± 0.22 mg/ml) (Table 8). DPPH test results were approved by the ABTS test results. Indeed the trans-2,5 dimethylpiperazine scavenging activity ($IC_{50}$= 0.97± 0.008 mg/ml) was approximatively thirteen time higher than the $(C_6H_{16}N_2)[CuCl_4]$ (13.73± 0.004mg/ml).

Our results showed that both trans-2,5 dimethylpiperazine and $(C_6H_{16}N_2)[CuCl_4]$ can be used as free radical scavenger substance. Nevertheless, both ABTS test and DPPH test revealed that trans-2,5 dimethylpiperazine –scavenging activity is significantly higher than the $(C_6H_{16}N_2)[CuCl_4]$. This result can be explained by the fact that the trans-2,5 dimethylpiperazine has a higher proton diffusion ability; furthermore, the trans-2,5 dimethylpiperazine structure contains more reactive sites, which could be proton donors or electron acceptors.

The disc diffusion method showed that, the effect of both the trans-2,5 dimethylpiperazine and $(C_6H_{16}N_2)[CuCl_4]$ dissolved in Dimethyl sulfoxide (DMSO) (1 mg/mL) on bacteria depended on membrane structure: gram positive or gram-negative bacteria (Table 9). Indeed, for gram-negative bacteria, the largest inhibition diameter (6.16 ± 0.26 mm) is recorded in *Pseudomonas aeruginosa* SH 38 by $(C_6H_{16}N_2)[CuCl_4]$. Moreover, the trans-2,5 dimethylpiperazine and $(C_6H_{16}N_2)[CuCl_4]$ have no observed effect on both *Escherichia coli* JW 1772 and *Salmonella typhimurium* ATCC 14028 where the inhibition zone does not exceed (6mm). However for the tested gram positive bacteria *Staphylococcus aureus* NCTC 6571 both the trans-2,5 dimethylpiperazine and $(C_6H_{16}N_2)[CuCl_4]$ were efficient. Statistical analysis showed that the the trans-2,5 dimethylpiperazine (9.83±0.28 mm) was more effective ($p$=0,015) against *Staphylococcus aureus* NCTC 6571 than the $(C_6H_{16}N_2)[CuCl_4]$ (8.33 ± 0.27mm) in Fig.17. Our results join many previous researches, where the antibacterial activity of newly synthesized compound depends on the membrane structure [**45**]. The difference of sensitivity, found between Gram-positive and Gram-negative bacteria to the the trans-2,5 dimethylpiperazine and our newly synthetized compound can be attributed to the outer membrane of Gram-negative bacteria that usually forms a physical barrier to most antibiotic. Indeed, for gram-negative bacteria the outer membrane permeability depends on many characteristics influencing the diffusion efficiency of the antibacterial compound via porins such us its polarity, lipophilicity and its size [**12**]. However, for Gram-positive bacteria, the diffusion of antibacterial agent is easier as the antibacterial agent target is the peptidoglycan layer and the inner membrane [**12**].

## 5. Conclusion

Finally, we have presented the synthesis and physicochemical characterization of the new compound $(C_6H_{16}N_2)[CuCl_4]$. The atomic arrangement can be described by thick layers of inorganic entities, made up from $CuCl_4$ anions, developed parallel to the (a, c) planes. The organic cations are anchored onto successive layers and connect them via N-H...Cl hydrogen bonds to form an infinite three dimensional network. Hirshfeld surface allowed us to investigate the stabilization of the crystal packing and to quantify the propensity of the intermolecular interactions to form the supramolecular assembly. The presence of functional groups of both anion and cation was proved by IR and Raman vibrational analysis and DFT theory. The optical properties were examined by experimental optical absorption and TDDFT calculation. The assignment of the observed electronic transitions reveals the formation of stable excitonic states and the occurrence of charge transfer within the inorganic sublattice. We also concluded the semiconductor behavior of this material and thus, the electrical

response was studied as a function of temperature and frequency. The AC conductivity was found to obey the universal power law. Moreover, the temperature dependence of conductivity was analyzed using the Arrhenius approach. Finally the bioassay results showed that the structure exhibits significant antibacterial activity.

## Supplementary data

Crystallographic data for the structural analysis have been deposited at the Cambridge Crystallographic Data Centre, N° de Cambridge: CCDC 1975728

**References**

[1] David B. Mitzi, Ph. Brock,Inorganic Chemistry 40 **(2001)** 2096-2104.

[2] S.V.Voitekhovich, A. S. Lyakhov, L. S. Ivashkevich, F. Schleife, R. Schnorr, B.Kersting, P. N. Gaponik, Inorg. Chim. Acta 419**(2014)** 124-129.

[3] K.Azouzi, B.Hamdi, R.Zouari. A.Ben Salah, Ionics 22 **(2016)** 1669-1680.

[4] Faist, J., Seebacher, W., Saf, R., Brun, R., Kaiser, M. & Weis, R.,J. Med. Chem. 47 **(2012)** 510–519.

[5] Kulig, K., Sapa, J., Maciag, D., Filipek, B. & Malawska, B. Arch. Pharm. Chem. Life Sci. 340 **(2007)**, 466–475.

[6] N. Drissi, K. Karoui, F. Jomni, A. Ben Rhaiem, Physica E: Low-dimensional Systems and Nanostructures 83 **(2016)** 349-357.

[7] A. Kessentini, M. Belhouchet, J.J. Suñol, Y. Abid, T. Mhiri, Journal of Luminescence 149 **(2014)** 341–347.

[8] G. M. Sheldrick, *Acta Cryst.*, (**2015**), *A71*, 3-8

[9] Diamond - Crystal and Molecular Structure Visualization, Crystal Impact - Dr. H. Putz &Dr.K.BrandenburgGbR,Kreuzherrenstr.102,53227Bonn,Germany.

[10] Brace, A., Tommasi, N.D., Bari, L.D., Pizza, C., Politi, M., Morelli, I. 2001. Antioxidant Principles from *Bauhinia terapotensis*. *Journal of Natural Products*. 64: 892–895.

[11] Hachani, A., Dridi, I., Elleuch, S., Roisnel, T., Kefi, R. **2019**. *Inorganic Chemistry Communications*. 100 : 134-143.

[12] Heesterbeek, D.A.C., Martin, N.I., Velthuizen, A., Duijst, M., Ruyken, M., Wubbolts, R., Rooijakkers, S.H.M., Bardoel, B.W. **2019**. 9:3074. https://doi.org/10.1038/s41598-019-38577-9.

[13] M.J. Frisch, G.W. Trucks, H.B. Schlegel, G.E. Scuseria, M.A. Robb, J.R. Cheeseman, G., GAUSSIAN 09, Revision A.1, GAUSSIAN, Inc, Wallingford CT (2009).

[14] A.D. Becke, Phys. Rev. 38 (1988) 3098-3100.

[15] A.D. Becke, J. Chem. Phys. 98 (1993) 1372-1377.

[16] C. Lee, W. Yang, R.G. Parr, Phys. Rev. B 37 (1988) 785-789.

[17] P.J. Hay, W.R. Wadt, J. Chem. Phys. 82 (1985) 270‑283.

[18] R. Dennington, T. Keith, J. Millam, GaussView, Version 5.0.8, Semichem Inc, Shawnee Mission KS, 2009.

[19] National Institute of Standards and Technology (NIST). Computational chemistry comparison and benchmark data base: Precomputed vibrationals caling factor

[20] C. Zanchini, R. D. Willett. Inorg. Chem., 29 (**1990**) 3027 – 303

[21] L. Yang, D. R. Powell, R. P. Houser, tau4, Dalton Trans, **(2007)** 955 - 964.

[22] I. Mkaouar, N. Karâa, B. Hamdi, R. Zouari, Journal of Molecular Structure 1115 (2016) 161-170.

[23] I. Mkaouar, B. Hamdi, N. Karaa, R. Zouari, Polyhedron 87 **(2015)** 424–432.

**[**24] J.J. McKinnon, M.A. Spackman, A.S. Mitchell, Acta Crystallogr. B B60**(2004)** 627–666.

[25] B. Guillot, E. Enrique, L. Huder, C. Jelsch, MoProViewer, Acta Cryst A70 (**2014**) C279.

[26] R. Mesbeh, A. Ben Ahmed, B. Hamdi, R. Zouari, Ionics 22 **(2016)** 2075- 2086

[27] A.Kessentini, M.Belhouchet, Y.Abid, C.Minot, T.Mhiri, Spectrochim Acta A 122 **(2013)** 476-481.

[28] Z.-L. Xiao, H.-Z. Chen, M.-M. Shi, G. Wu, R.-J. Zhou, Z.-S. Yang, M. Wang, B.-Z. Tang, Materials Science and Engineering B 117 (2005) 313–316.

[29] Y.-Y. Zheng, G. Wu, M. Deng, H.-Z. Chen, M. Wang, B.-Z. Tang, Thin Solid Films 514 (2006) 127–131.

[30] X.-W. Pan, G. Wu, M. Wang, H.-Z. Chen, Zhejiang Univ Sci A 2009 10(5) 710-715.

[31] T. Dammak, H. Boughzala, A. Mlayah, Y. Abid, Journal of Luminescence 173 (2016) 213–217.

[32] A. Jellali, B. Hamdi, N. Salah, R. Zouari, Journal of Inorganic and Organometallic Polymers and Materials (2018) DOI: 10.1007/s10904-018-0822-y.

[33] W. Wang, X. Chen, S. Efrima, Chem. Mater. 11 (1999) 1883-1889.

[34] E. Shikoh, Y. Ando, M. Era, T. Miyazaki, Journal of Magnetism and Magnetic Materials 226-230 (2001) 2021-2022.

[35] C. Aruta, F. Licci, A. Zappettini, F. Bolzoni, F. Rastelli, P. Ferro, T. Besagni, Appl. Phys. A 81 (2005) 963-968.

[36] M. M. Alam, F.O. Lucas, D. Danieluk, A.L. Bradley, K.V. Rajani, S. Daniels and P.J. McNally, J. Phys. D: Appl. Phys. 42 (2009) 225307.

[37] H. Sies, Experimental Physiologv, 82 (1997) 291-295.

[38] M. Valko, D. Leibfritz, J. Moncol, M.T.D. Cronin, M. Mazur, J. Telser,. J.Biochem. Cell Biol. 39 **(2007)** 44–84.

[39] L.R. Domingo, M. Ríos-Gutiérrez, P. Pérez, Molecules 2016, 21, 748.

[40] A. Veved, G.W. Ejuh, N. Djongyang, Polymer Bulletin, https://doi.org/10.1007/s00289-020-03346-6.

[41] Z.L. Wang, L.H. Wei, L.Y. Jin, J.P. Wang, Chin. J. Struct. Chem. 26 (**2007**) 1423–1428.

[42] H. Chouaib, S. Kamoun, , J. Phys. Chem. Solids, 85 **(2015)** 218.

[43] R. Elwej, M. Hamdi, N. Hannachi, F. Hlel.Mater. Res. Bull, 62 **(2015)** 42.

[44] Z. Ouerghi et al , Journal of Molecular Structure 1173 **(2018)** 439e447.

[45] I. Wacharine, A. Valkonen, M. Rzaigui, W. Smirani, *Monatsh. Chem*, 146 **(2015)** 2007.

## Figure captions

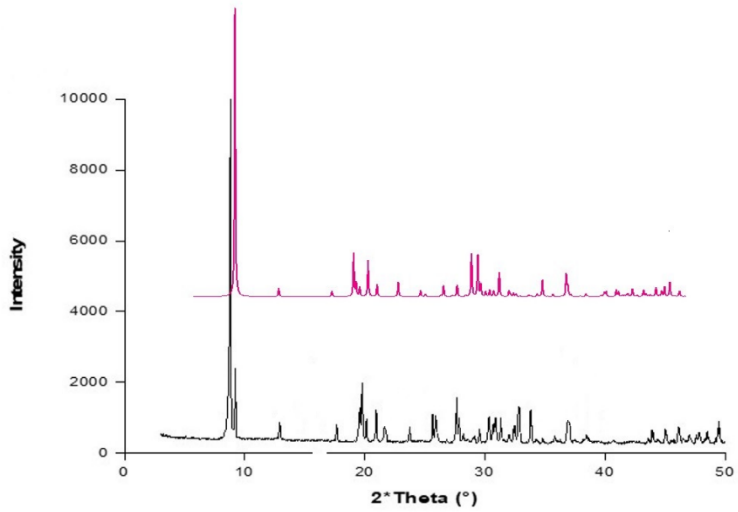


**Fig.1: Experimental (black) and simulated (pink) powder XRD patterns of $(C_6H_{16}N_2)[CuCl_4]$.**

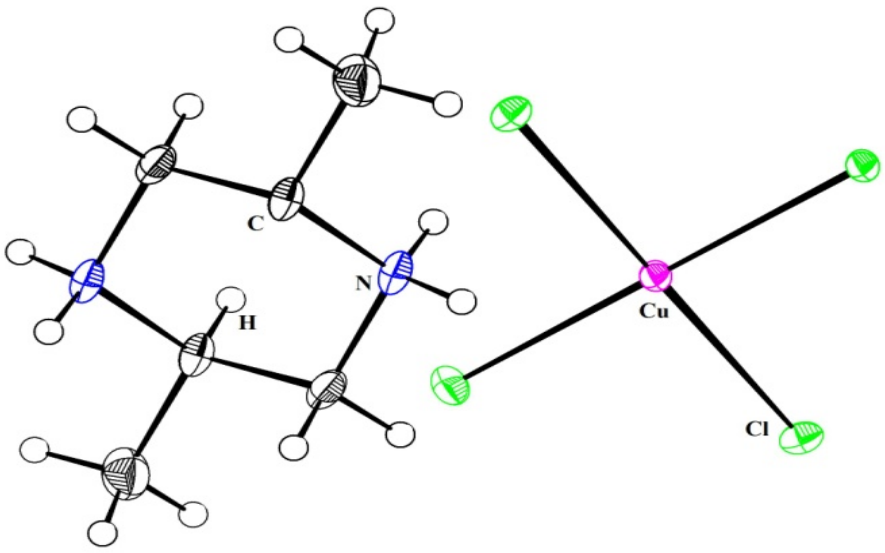


**Fig.2: ORTEP view of the asymmetric unit of the $(C_6H_{16}N_2)[CuCl_4]$.**

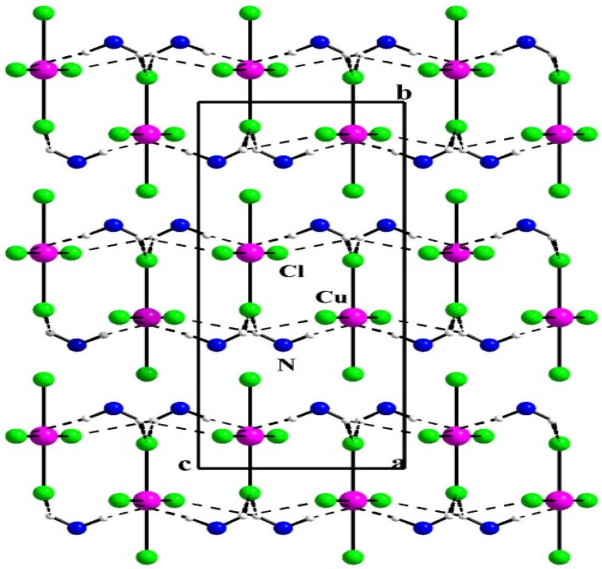


**Fig.3: View along the [100] direction of an inorganic layer of the title compound**

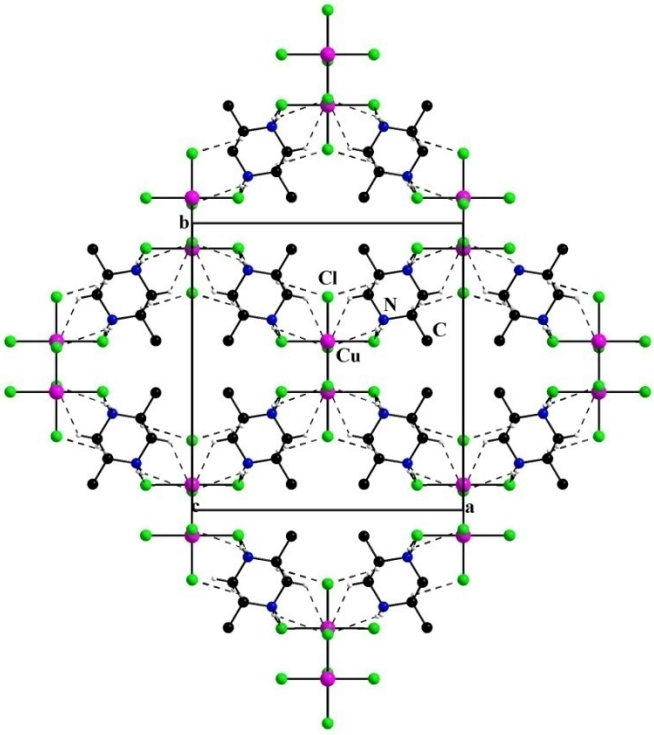


**Fig.4: View along the [001] direction showing the three dimensional network of $(C_6H_{16}N_2)[CuCl_4]$**

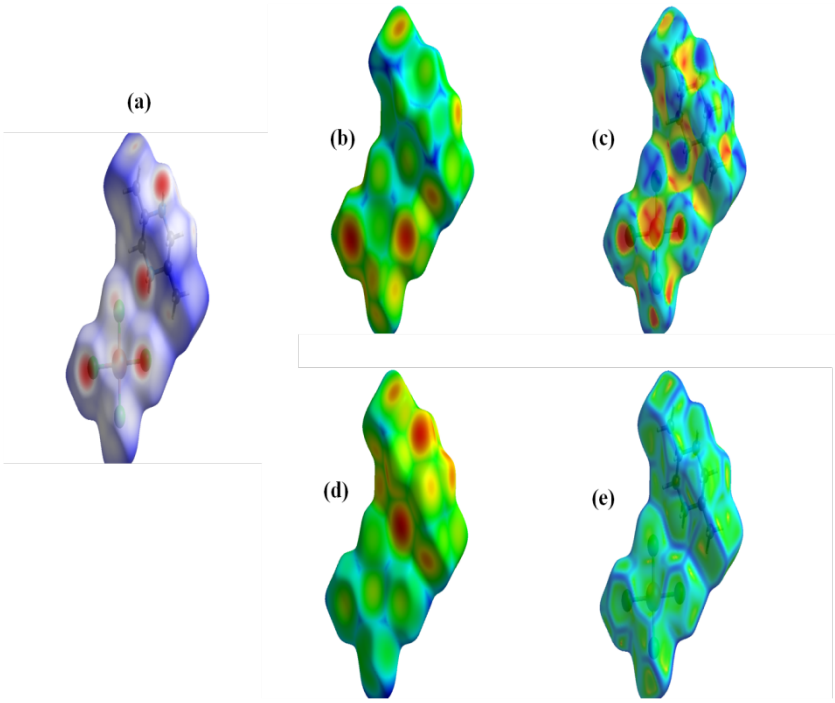


**Fig.5: Hirshfeld surface analysis of $(C_6H_{16}N_2)[CuCl_4]$. (a) dnorm, (b) de, (c) shape-index, (d) di, (e) curvedness.**

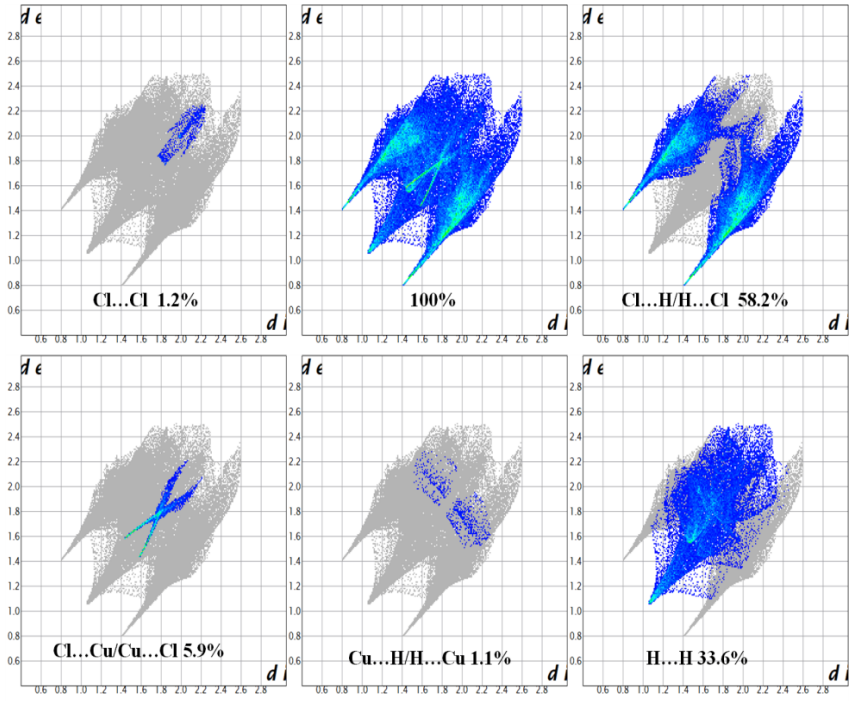


**Fig.6: Fingerprint plots of contacts in $(C_6H_{16}N_2)[CuCl_4]$.**

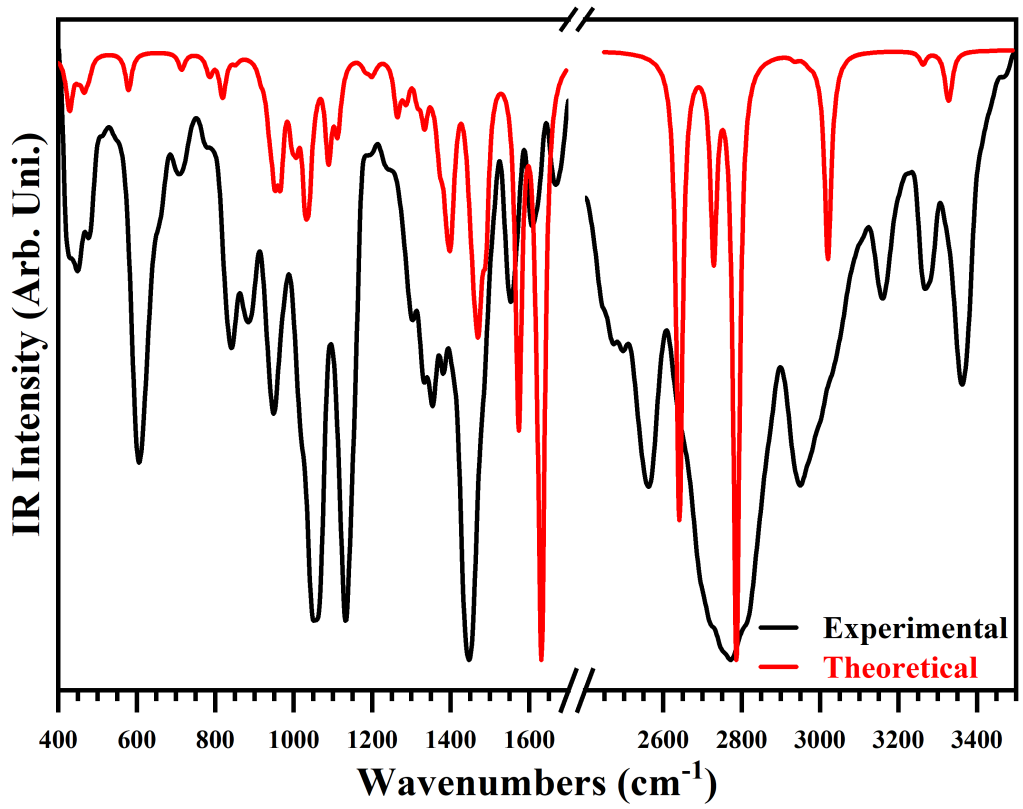


**Fig.7: Experimental (black) and theoretical (red) IR spectra of $(C_6H_{16}N_2)[CuCl_4]$.**

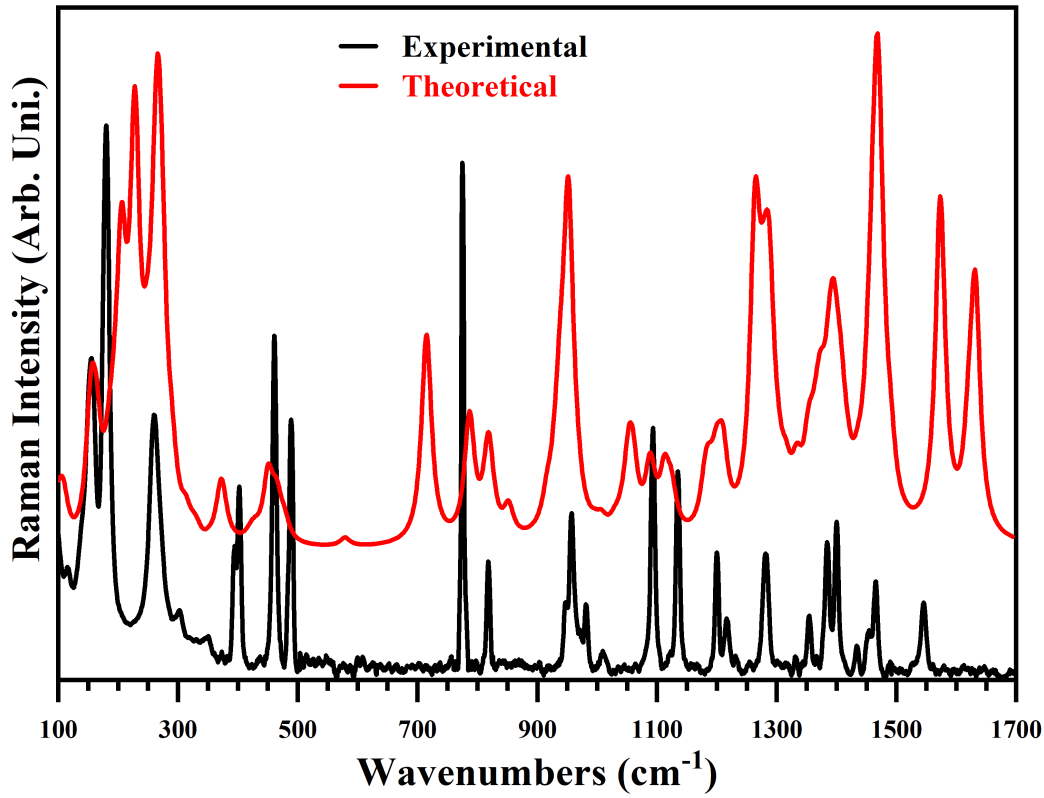


**Fig.8: Experimental (black) and theoretical (red) Raman spectra of $(C_6H_{16}N_2)[CuCl_4]$.**

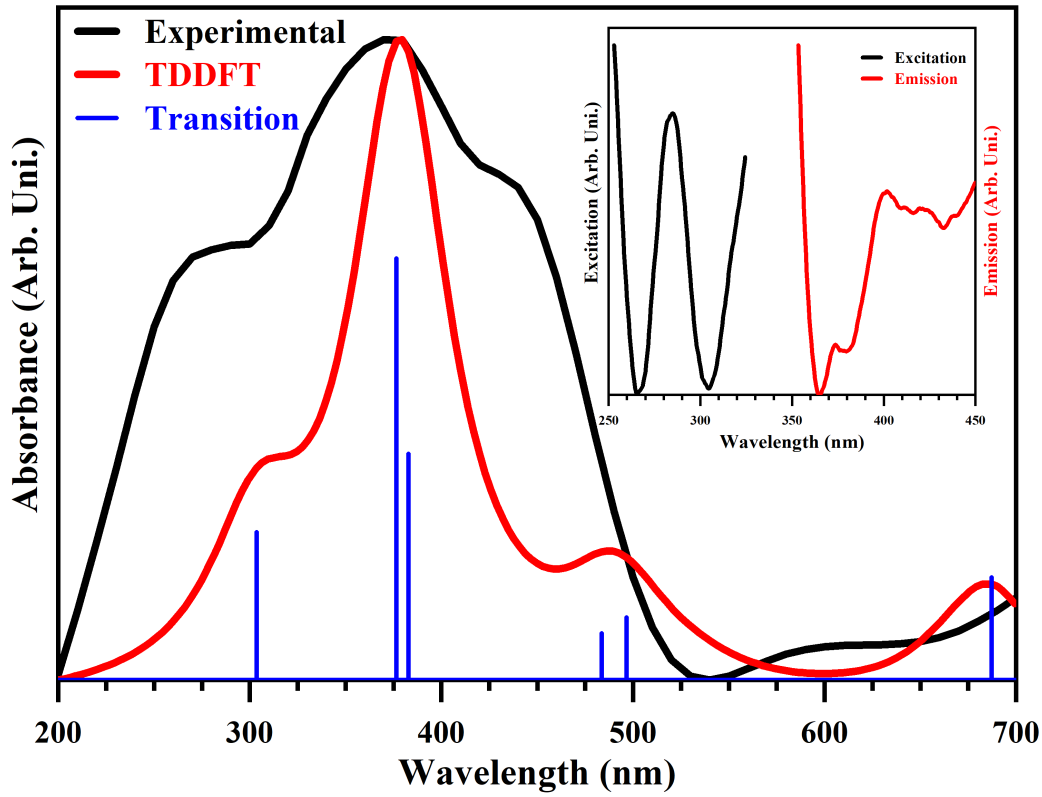


**Fig.9: Optical properties of $(C_6H_{16}N_2)[CuCl_4]$: experimental (black) and theoretical (red) Absorption spectra. In the inset: Excitation (black) and Emission (red) spectra.**

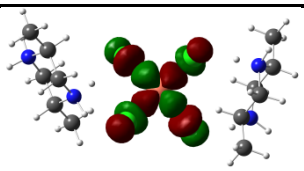

**LUMO (E=-9.29 eV)**

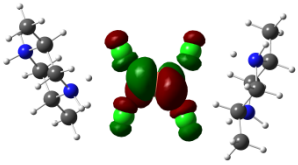

**HOMO (E=-11.73 eV)**

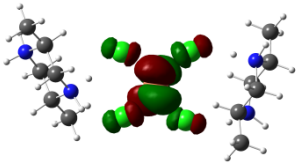

**HOMO-1**

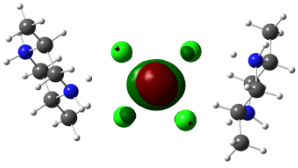

**HOMO-2**

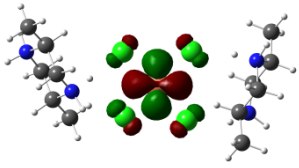

**HOMO-3**

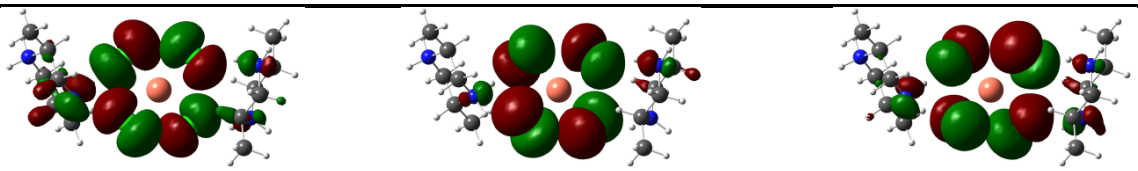


**Fig.10: representation of some frontier molecular orbitals of $(C_6H_{16}N_2)[CuCl_4]$.**

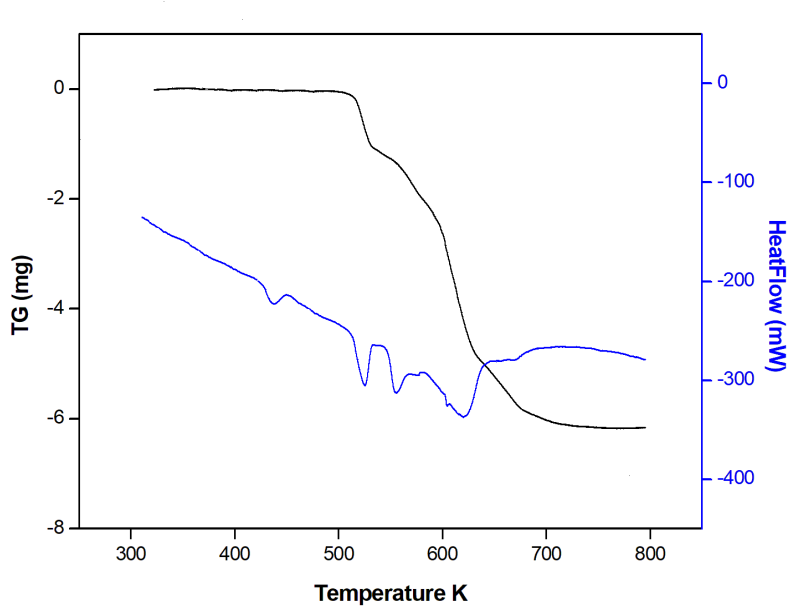


**Fig.11: TG-DTA heating of $(C_6H_{16}N_2)[CuCl_4]$.**

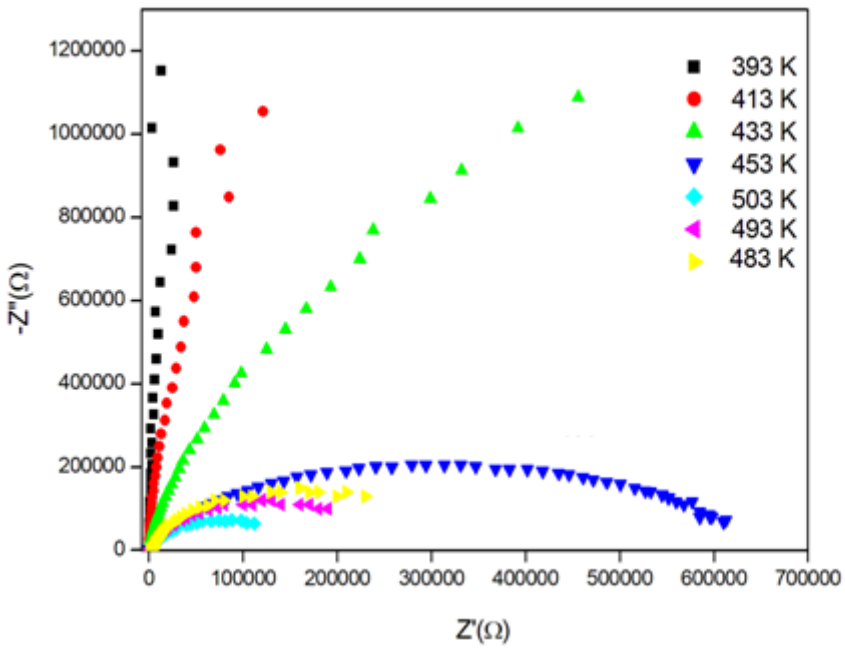

**Fig.12: Complex impedance diagrams (- Z'' vs Z') for $(C_6H_{16}N_2)[CuCl_4]$ at various temperatures.**

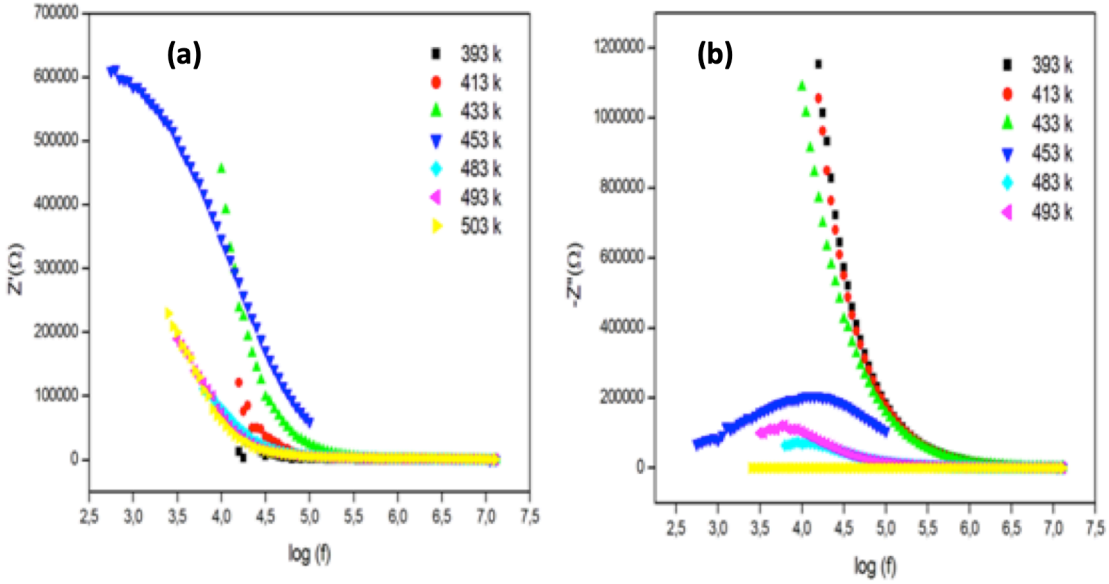


**Fig.13: Plots of the real and imaginary parts of impedance Z' (a) and Z'' (b) vs. log(f) of $(C_6H_{16}N_2)[CuCl_4]$ at various temperatures.**

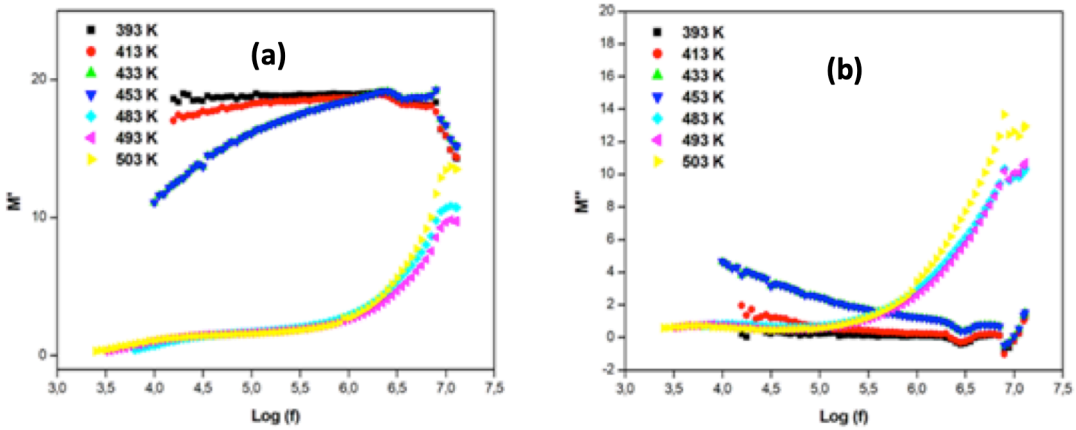


**Fig.14: Variation of the real M' (a) and imaginary parts M'' (b) of the electric modulus as a function of the frequency at various temperatures in $(C_6H_{16}N_2)[CuCl_4]$.**

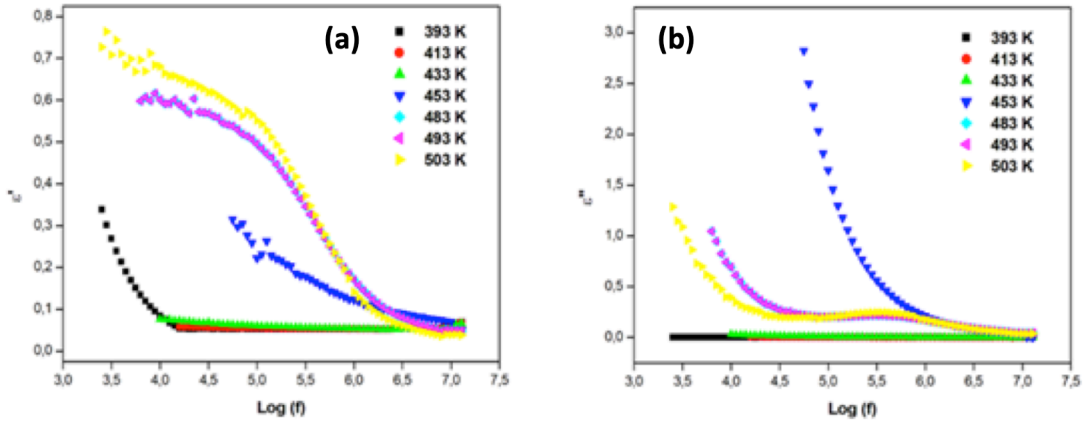


**Fig.15: Variation of the real ε'(a) and imaginary parts ε'' (b) as a function of the frequency at various temperatures in $(C_6H_{16}N_2)[CuCl_4]$.**

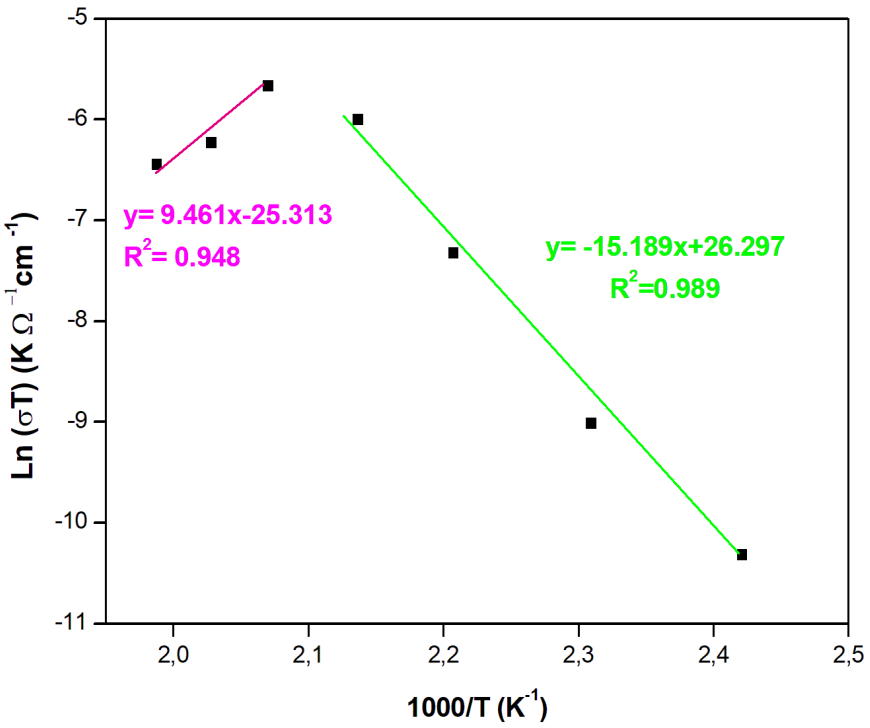


**Fig.16: Ln (σT) as a function of 1000/T.**

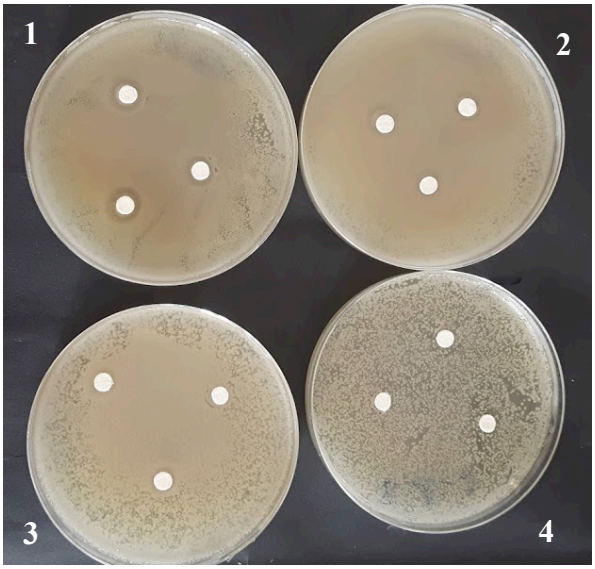


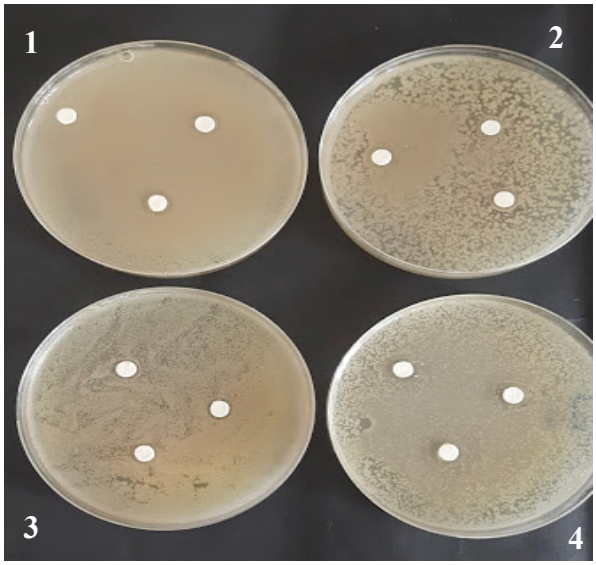


$(C_6H_{16}N_2)$ $[CuCl_4]$ Trans-2,5 dimethylpiperazine

**Fig.17: Zone of inhibition (mm), caused by the $(C_6H_{16}N_2)[CuCl_4]$ and the trans-2,5dimethylpiperazine against bacteria: 1:Pseudomonas aeruginosa, 2: Escherichia coli, 3: Staphylococcus aureus, 4: Salmonella typhimurium**

**Table 1: Summary of crystal data, intensity measurements, and refined parameters for $(C_6H_{16}N_2)[CuCl_4]$.**

| | |
|---|---|
| **Crystal data** | |
| Chemical formula | $(C_6H_{16}N_2)$ $[CuCl_4]$ |
| *M*r | 321.55 |
| Crystal system | Monoclinic |
| Space group | C2/c |
| Temperature (K) | 150 |
| *a*, *b*, *c* (Å) | 14.500 (5), 14.619 (5), 5.9173 (17) |
| *β* (°) | 107.419 (11) |
| *V* (Å$^3$) | 1196.8 (7) |
| *Z* | 4 |
| Radiation type | Mo *Kα* |
| *μ* (mm$^{-1}$) | 2.677 |
| Crystal size (mm) | 0.58 × 0.12 × 0.09 |
| Crystal color | Yellow |
| **Data collection** | |
| Diffractometer | D8 VENTURE Bruker AXS |
| Absorption correction | Multi-scan |
| *T*min, *T*max | 0.786, 0.551 |
| No. of measured, independent and observed [*I* 2*σ*(*I*)] reflections | 5782, 1367, 1230 |
| *R*int | 0.058 |
| **Refinement** | |
| *R* [$F^2$> 2*σ*($F^2$)], *wR*($F^2$), *S* | 0.026, 0.068, 1.06 |
| No. of parameters | 69 |
| Δ*ρ*max, Δ*ρ*min (e Å$^{-3}$) | 0.40, −0.41 |

**Table 2: Hydrogen-bond geometry (Å, º) in $(C_6H_{16}N_2)[CuCl_4]$.**

| D-H…A | D-H | H…A | D…A | D-H…A |
|---|---|---|---|---|
| C1— H1A...Cl1_#1 | 0.99 | 2.95 | 3.5995 (19) | 123.8 |
| C1— H1A ...Cl3 | 0.99 | 2.75 | 3.394 (2) | 122.9 |
| N2— H2A...Cl2_#2 | 0.88 (2) | 2.40(2) | 3.2084(19) | 153.3(19) |
| N2— H2A...Cl3 | 0.88 (2) | 2.76(2) | 3.1756(17) | 110.7(16) |
| N2 —H2B...Cl2_#3 | 0.90 (2) | 2.29(2) | 3.1850(18) | 171(2) |
| C3 —H3...Cl1_#4 | 1.00 | 2.83 | 3.4555(18) | 121.3 |

Symmetry transformations used to generate equivalent atoms:

#1 -x, -y, -z T = [1, 1, 1]

#2 x, -y, z-1/2 T = [0, 1, 0]

#3 x, -y, z-1/2 T = [0, 1, 1]

#4 x+1/2, y+1/2, z T = [0, 0, 0]

**Table 3: Geometric parameter (º) in $(C_6H_{16}N_2)[CuCl_4]$.**

| **Distance (Å)** | | **Angle (°)** | |
|---|---|---|---|
| Cu1—Cl1 | 2.2610 (10) | Cl1—Cu1—Cl3 | 180.0 |
| Cu1—Cl3 | 2.2772 (10) | Cl1—Cu1—Cl2 | 90.164 (11) |
| Cu1—Cl2 | 2.3585 (8) | Cl3—Cu1—Cl2 | 89.836 (11) |
| Cu1—Cl2ii | 2.3585 (9) | Cl1—Cu1—Cl2ii | 90.164 (11) |
| C1—N2 | 1.498 (2) | Cl3—Cu1—Cl2ii | 89.836 (11) |
| C1—C3i | 1.512 (2) | Cl2—Cu1—Cl2ii | 179.67 (2) |
| N2—C3 | 1.497 (2) | N2—C1—C3i | 111.66 (15) |
| C3—C4 | 1.513 (3) | C3—N2—C1 | 111.04 (14) |
| **Dihedral (°)** | | N2—C3—C1i | 109.41 (14) |
| C3—C1i—N2—C3 | -57.60 (19) | N2—C3—C4 | 110.14 (15) |
| C1— N2—C3—C1i | 56.3 (2) | C1—C3—C4 | 110.88 (16) |
| C1— N2—C3— C4 | 178.43 (16) | | |

Symmetry code: (i) $-x+3/2, -y+3/2, -z+1$ ; (ii) $-x+1, y, -z+1/2$ .

**Table 4: The chemical nature of contacts in the crystal structure of $(C_6H_{16}N_2)[CuCl_4]$.**

| **Enrichment** | **C** | **N** | **Cl** | **Cu** | **HC** | **HN** |
|---|---|---|---|---|---|---|
| **C** | 5.20 | | | | | |
| **N** | 18.01 | 0.00 | | | | |
| **Cl** | 0.12 | 0.00 | 0.52 | | | |
| **Cu** | 0.20 | 0.00 | **0.89** | 2.83 | | |
| **HC** | 0.52 | 0.00 | **1.08** | 0.06 | **2.10** | |
| **HN** | 0.15 | 0.00 | **2.80** | 0.26 | 0.19 | 0.00 |
| **Surface %** | 14.83 | 0.69 | **25.85** | 2.4 | **47.00** | **9.48** |

**Table 5: Assignments of IR and Raman vibrational modes in $(C_6H_{16}N_2)[CuCl_4]$.**

| Infrared | | Raman | | Assignments |
|---|---|---|---|---|
| **Experimental** | **Theoretical** | **Experimental** | **Theoretical** | |
| 3361 | 3327 | | | $\nu_{as}$ ($NH_2$) |
| 3268 | 3262 | | | $\nu_s$ ($NH_2$) |
| 3158 | 3020 | | | $\nu_{as}$ ($CH_2$) |
| 2948 | | | | $\nu_{as}$ ($CH_3$) |
| 2771 | 2786 | | | $\nu_s$ ($CH_2$) |
| 2722 | 2728 | | | $\nu_s$ ($CH_3$) |
| 2561 | 2641 | | | ν (NH…Cl) |
| 1668 | 1631 | | 1629 | δ ($NH_2$), δ ($CH_2$) |
| 1552 | 1573 | 1545 | 1573 | |
| | | 1526 | | |
| | 1486 | 1488 | | ω ($NH_2$) |
| | 1469 | 1464 | 1468 | δas ($CH_3$) |
| 1448 | | 1454 | | |
| | | 1433 | | |
| | 1398 | 1399 | 1394 | δs ($CH_3$) |
| 1380 | 1376 sh | 1383 | 1375 sh | δ (CH) |
| 1353 | | 1354 | 1355 sh | ω ($CH_2$) |

| | | | | |
|---|---|---|---|---|
| 1332 | 1333 | 1330 | 1334 | t ($NH_2$), t ($CH_2$) |
| | 1318 | 1315 | 1316 | |
| 1303 | | 1300 | | |
| | 1285 | 1281 | 1284 | |
| 1243 | 1264 | 1254 | 1265 | |
| | | 1231 | | |
| | | 1216 | | |
| 1191 | 1199 | 1200 | 1205 | |
| | 1184 | | 1184 | |
| 1132 | 1110 | 1134 | 1113 | |
| | 1089 | 1093 | 1089 | |
| 1054 | 1033 | | 1055 | ν (CC), ν (CN) |
| 1024 sh | 1005 | 1009 | 1004 | |
| | 964 | 981 | | |
| 948 | 952 | 957 | 951 | ρ ($NH_2$) |
| 883 | 916 sh | 947 sh | | ν (CN) |
| 840 | 850 | | 850 | ρ ($CH_3$), ρ ($CH_2$) |
| | 818 | 818 | 818 | |
| 781 | 785 | 771 | 787 | |
| 709 | 714 | | 715 | δ ring |
| 605 | 579 | 604 | 579 | |
| 476 | 467 | 488 | 466 | |
| 446 | | 460 | 451 | |
| 426 | 429 | 402 | 426 | |
| | 372 | 394 | 373 | |
| | 324 | 302 | 310 sh | |
| | 270 | 260 | 266 | $\nu_{as}$ (CuCl) |
| | | | 227 | τ ($CH_3$) |
| | 195 | 180 | 206 | $\nu_s$ (CuCl) |
| | 159 | 155 | 157 | δas (CuCl) |
| | 96 | 115 | 104 | δs (CuCl) |

**Table 6: Experimental and TDDFT computed electronic transitions in ($C_6H_{16}N_2$)[$CuCl_4$].**

| Experimental | Theoretical | | | |
|---|---|---|---|---|
| **Wavelength (nm)** | **Wavelength (nm)** | **Transition (nm)** | **Oscillator strength** | **Nature (%)** |
| 630 | 687 | 687.18 | 0.0271 | H → L (25%) |
| 430 | 486 | 496.56 | 0.0165 | H-1 → L (30%) |
| | | 483.63 | 0.0123 | H-2 → L (13%) |
| 373 | 379 | 382.82 | 0.0597 | H-3 → L (11%) |
| | | 376.47 | 0.1114 | H-4 → L (32%) |
| 285 | 303 | 303.50 | 0.039 | H-5 → L (21%), |

**Table7: The calculated HOMO, LUMO, energy values, HOMO-LUMO, energy gap, chemical potential, chemical hardness, electrophilicity index and softness of the compound.**

| Parameters | Values (eV) |
|---|---|

| | |
|---|---|
| $E_{HOMO}$ | -11.73 |
| $E_{LUMO}$ | -9.29 |
| Energy band gap $\lvert E_{HOMO}-E_{LUMO}\rvert$ | 2.44 |
| Chemical hardness $\eta = \frac{(I-A)}{2}$ | 1.22 |
| Chemical potential for the molecule $\mu = \frac{-(I+A)}{2}$ | -10.51 |
| The softness $S = \frac{1}{2\eta}$ | 0.409 |
| Electrophilicity index of the molecule $W = \frac{\mu^2}{2\eta}$ | 45.27 |

**Table 8: Scavenging activity of trans-2,5 dimethylpiperazine and $(C_6H_{16}N_2)[CuCl_4]$ in both DPPH and ABTS test.**

| | DPPH ($IC_{50}$ mg/ml) | ABTS ($IC_{50}$ µg/ml) |
|---|---|---|
| $(C_6H_{16}N_2)$ $[CuCl_4]$ | 49.2± 0.22*** | 13.73± 0.03*** |
| trans-2,5 dimethylpiperazine | 1.83± 0.06 | 0.97± 0.02 |

The data are reported as mean ± standard deviation, *** $p<0.001$ significantly different from the trans-2,5 dimethylpiperazine.

**Table 9: Inhibition zone (mm), caused by the trans-2,5 dimethylpiperazine and $(C_6H_{16}N_2)$ $[CuCl_4]$ against bacteria.**

| | Inhibition Zone (mm) | |
|---|---|---|
| **Bacteria** | **$(C_6H_{16}N_2)$ $[CuCl_4]$** | **trans-2,5 dimethylpiperazine** |
| *Pseudomonas aeruginosa* SH 38 | 6.16 ± 0.26 | 6 |
| *Escherichia coli* JW 1772 | 6 | 6 |
| *Salmonella typhimurium* ATCC 14028 | 6 | 6 |
| *Staphylococcus aureus* NCTC 6571 | 8.33±0.27 | 9.83±0.28* |

The data are reported as mean ± standard deviation. * $p<0.05$: significantly different from the compound.

## Highlights

- Synthesis of new organic-inorganic hybrid material $(C_6H_{16}N_2)[CuCl_4]$
- The determination of crystallographic coordinates by XRD on a crystal.
- Study the different properties (vibrational, optical) , DFT and TDFT calculations.
- The temperature dependence of conductivity was analyzed using the Arrhenius approach.
- The bioassay results showed that the structure exhibits significant antibacterial activity.

**Supplementary :**

**S1: the Correlation graph between the experimental and calculated vibrationnal wavenumbers (cm−1).**

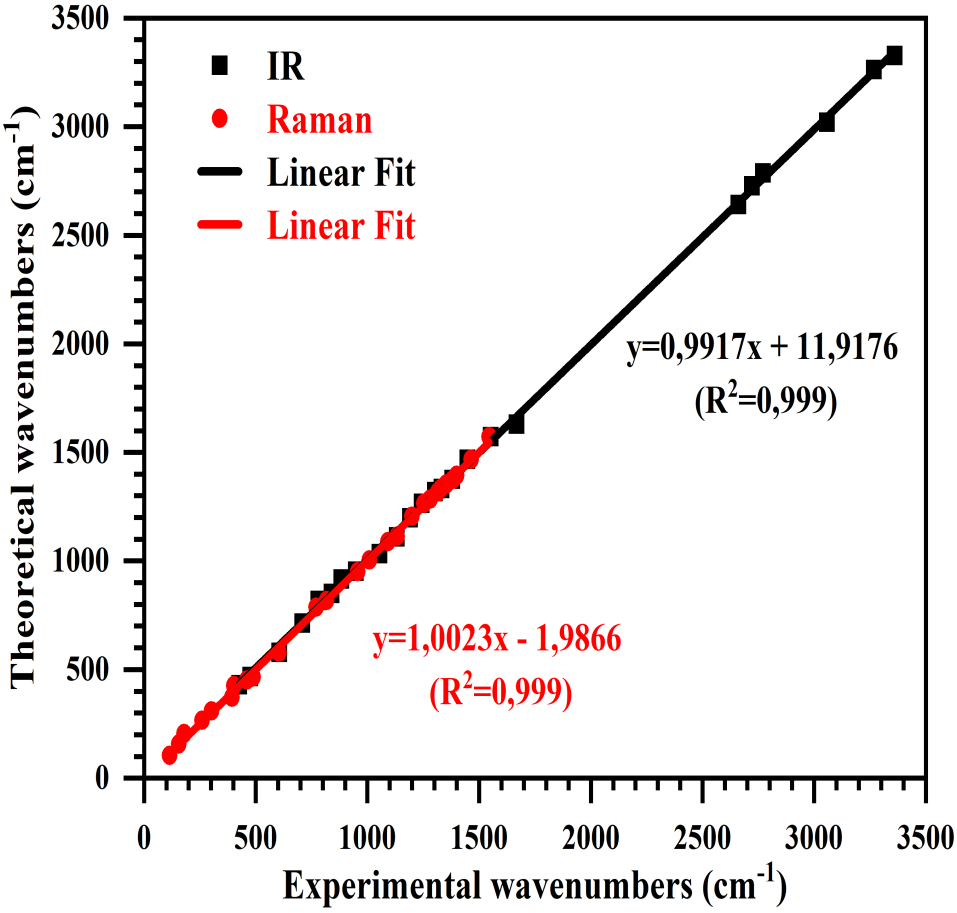

**S2: Tthe trauc plot of the $(C_6H_{16}N_2)$ [$CuCl_4$] compound**

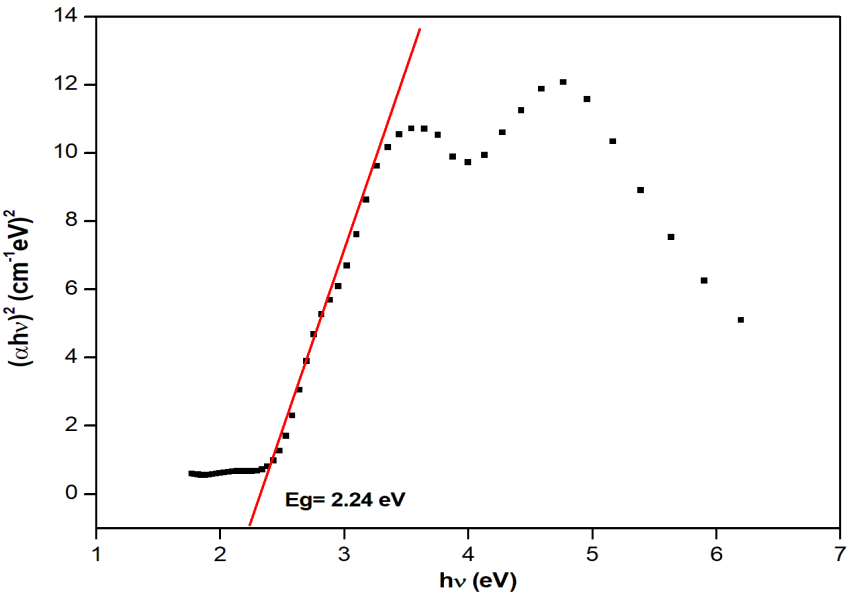


**S3: DSC curve for $(C_6H_{16}N_2)$ [$CuCl_4$]**